

Mechanics-Informed Autoencoder Enables Automated Detection and Localization of Unforeseen Structural Damage

Xuyang Li[✉], Hamed Bolandi[✉], Mahdi Masmoudi[✉], Talal Salem[✉], Nizar Lajnef[✉], and Vishnu Naresh Boddeti[✉]
Michigan State University, East Lansing, MI 48824, USA

(Dated: February 26, 2024)

Structural health monitoring (SHM) is vital for ensuring the safety and longevity of structures like buildings and bridges. As the volume and scale of structures and the impact of their failure continue to grow, there is a dire need for SHM techniques that are scalable, inexpensive, operate passively without human intervention, and customized for each mechanical structure without the need for complex baseline models. We present a novel “deploy-and-forget” approach for automated detection and localization of damages in structures. It is based on a synergistic combination of fully passive measurements from inexpensive sensors and a mechanics-informed autoencoder. Once deployed, our solution continuously learns and adapts a bespoke baseline model for each structure, learning from its undamaged state’s response characteristics. After learning from just 3 hours of data, it can autonomously detect and localize different types of unforeseen damage. Results from numerical simulations and experiments indicate that incorporating the mechanical characteristics into the variational autoencoder allows for up to 35% earlier detection and localization of damage over a standard autoencoder. Our approach holds substantial promise for a significant reduction in human intervention and inspection costs and enables proactive and preventive maintenance strategies, thus extending the lifespan, reliability, and sustainability of civil infrastructures.

INTRODUCTION

Structural health monitoring plays an important role in monitoring and ensuring the safety and reliability of various engineering systems. Poor monitoring and maintenance can lead to serious damage or even catastrophic failures of structures. Despite the effort of frequent manual inspections and the installation of many active sensors over the years, numerous structural failures have been witnessed. For instance, a serious crack in the I-40 Bridge in Memphis went undetected for years before being discovered in 2021 [1], resulting in long-term road closure, substantial economic losses, and significant safety concerns among the public. Similarly, in 2022, a bridge in Pittsburgh collapsed due to the corrosion and deterioration at the bridge legs [2], damaging several vehicles and many injuries. Preventing such incidents as the built environment scales and ages necessitates the development of passive, inexpensive, and continuous structural monitoring techniques, with the ultimate aim of detecting, localizing, and identifying types of damages at an early stage. Such solutions would complement existing active, and costly manual inspections.

Traditional SHM systems often employ various sensors to measure physical quantities such as strain, vibration, temperature, and acoustic emission, providing more details about the structure’s health condition. However, existing solutions either need active measurements [3–7], do not localize damage [5, 6, 8–13], or employ a very complex and expensive but accurate methodology [3, 4, 8].

Recently, many Machine Learning (ML) methods have emerged as potential enhancements, capable of extracting features from large amounts of sensor data. For example, significant efforts have been focused on utiliz-

ing sensor data to detect damages in gusset plates [14–17], bridges [18–20], highway sections [21], and railways [22, 23]. A support vector machine (SVM) was used to process sensor data and detect fatigue cracking in steel bridge structures [24]. Neural network-based classifiers were trained to identify damages in buildings [25], concrete slabs [9], pavement [26], and steel frames [10]. Several sequence-based models, such as recurrent neural networks [27] and long short-term memory (LSTM) and gated recurrent units [28], tried to utilize the time-series features from data to detect, localize, and quantify structural defects. The key of these approaches lies in their need for labeled sensor data corresponding to normal and damaged operating conditions, and are typically constrained by the availability of data annotations, which do not generalize to unseen damage scenarios. Many unsupervised anomaly detection approaches have also been developed with a focus on autoencoders [29, 30] and principal component analysis (PCA) [13, 31–33]. Besides detecting damages, a few ML approaches focus on damage localization with finite element model updating [34], convolutional neural network (CNN) [35, 36], and autoencoders [37].

However, in contrast to the extensive attention given to various damage detection and localization techniques, relatively limited efforts are focused on emerging damages in the early stage. Studies have utilized PCA-based approaches [38, 39], Gaussian mixture models [8], and autoencoders [40] exclusively for early damage detection. And there has been a notable absence of research dedicated to the development of automated, real-time SHM systems for early damage localization. To our knowledge, this is the first paper to emphasize both the automated detection and localization of early-stage damages. In addition, it is worth mentioning that while advanced ac-

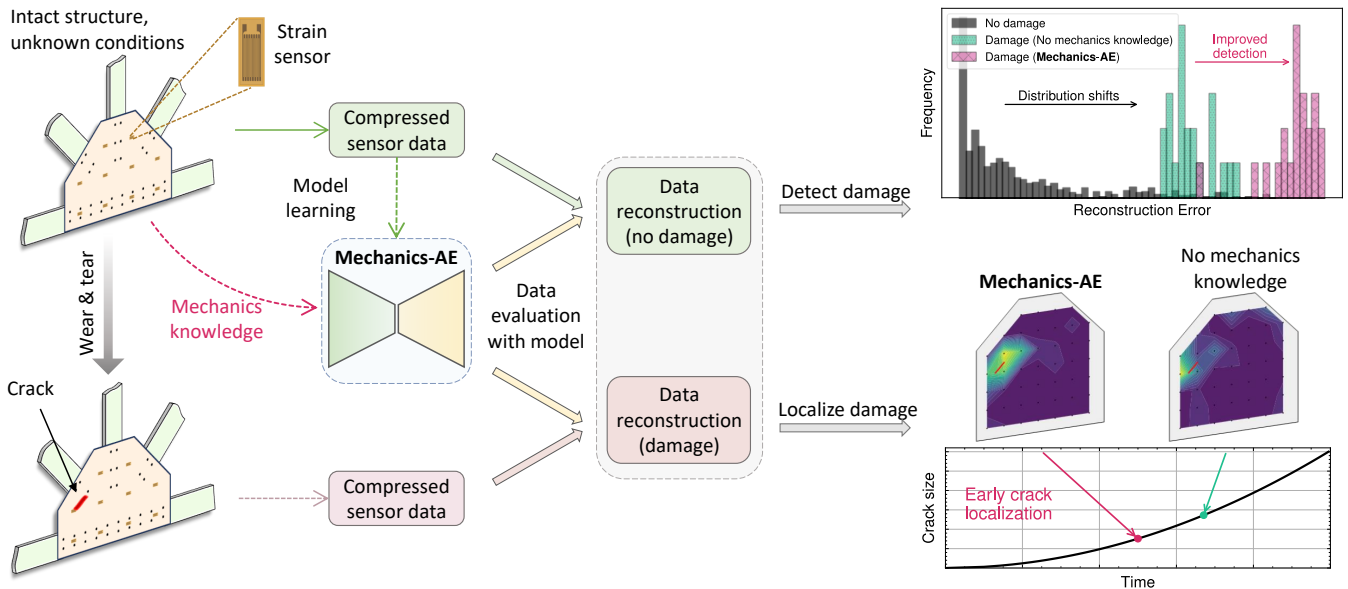


FIG. 1. **Overview of the automated structural damage detection and localization framework.** We train Mechanics-AE on a representative dataset of normal service structural operation response, and efficiently reduce the raw sensor data stream for network training. The properties of damage are unknown/undefined during training. Once trained, the reconstruction errors between the network’s input and output are used to construct a model reference representing the intact structural pattern. Data collected from the damaged structure are tested in the trained model. In the top right section of the figure, the observable shift in reconstruction errors effectively highlights the detection of anomalies indicative of damage. The incorporated mechanics knowledge notably enhances the distribution shift, leading to significant improvements in damage detection rate and the potential for early damage detection. In the bottom right section, we performed sensor-wise error comparisons based on norm value and displayed it in a contour. This process assists in early localization of anomalies representing the onset of damage.

tive sensing technologies like guided wave [5, 41, 42] and acoustic emission [6, 7] might offer improved accuracy for early-stage damage detection and localization, a notable challenge lies in their sophisticated operations, their inability to achieve automated real-time monitoring, and the need for complex baseline behavior models (such as finite element models).

Besides modern applications from ML, those computational methods present a number of unique challenges to existing SHM solutions due to the complexity and diversity of structures, sensors, and damage scenarios. First, the damage may be small, hidden, or distributed in the structure, making it difficult to early detect and localize using conventional methods based on predefined damage features or thresholds [43, 44]. Second, the damage may be unknown or novel, meaning that no prior knowledge or labeled data is available for training supervised learning models [26, 45] that can recognize the damage patterns. Third, employing multiple sensors over different locations on the structure is typical. However, existing methods [37, 46] are typically designed to model data from a single sensor or do not take the domain attributes of the structure and the sensor placement into account when detecting or localizing damage.

In this work, we propose Mechanics-AE, a real-time SHM framework for automated damage detection and

localization based on anomaly detection. Our approach utilizes a deep autoencoder that considers the mechanics relations in strain responses between each pair of sensors. Data collected from instrumented structures is used to establish the reference (baseline) for anomaly detection. In our case, we use the gusset plate as a typical example and assume that the sensor data collected from the plate during its normal operation represents the normal behavior of the structure, and any deviation from this behavior indicates potential damage. Therefore, we train Mechanics-AE in an unsupervised manner on the normal sensor data, aiming to reconstruct the input. Then Mechanics-AE can detect and localize anomalies from the test data. This approach enables our system to adapt to diverse structures and detect known and unknown anomalies without the need for any other models knowledge. More importantly, because sensor data is highly compressed (reduced), variations due to environmental or loading fluctuations are filtered out since they are already taken into account in the training data. Therefore, the recurrence of anomaly patterns is indicative of damage. Figure 1 shows the overview of the proposed novel mechanics-integrated unsupervised learning approach for the detection and localization of structural anomalies. The deep neural network contains a latent representation for data reconstruction and feature extraction. The

autoencoder integrates the mechanics knowledge based on different sensors’ strain responses. The detection approach is achieved by comparing the reconstruction discrepancies of the anomalies and normal data. And the localization approach takes a further step by computing the reconstruction errors concerning each sensor and representing them as contours. This approach does not require the use of any damaged instances of data for training, which is a significant advantage of our method given that it is practically impossible to collect realistic damaged data on large scale structures. Other techniques that use simulated damage scenarios often prove inaccurate and impractical for real-time applications due to the need for constant re-calibration. In contrast, our approach in this paper relies solely on reference data to establish an intact model reference and detect anomalies by tracking deviations from this reference. Furthermore, with the integrated mechanics knowledge, Mechanics-AE significantly improves its performance in detecting and localizing damages at an early stage of damage growth.

RESULTS

Establish reference structure behavior baseline

In this example, we use gusset plate-like geometries to showcase the effectiveness of our SHM solution. The approach can be extended to structural components. First, an intact (undamaged) polygon shape plate is analyzed with finite element simulations, and the mesh details are shown in Fig. 2a. This undamaged plate is subject to random traffic loads to represent the normal operations of a structural component. The detailed size of the plate is shown in Fig. 2b (thickness is 1.2cm). Strain responses are measured from 45 points within the structure and are marked in Fig. 2b. The time-series data are extracted, segmented, and then compressed based on Gaussian distributions, with detailed information provided in the Method Section. The compressed data consists of μ and σ values for each sensor in the time sequence. Subsequently, the Mechanics-AE model utilizes this data for training, to reconstruct the input compressed sensor data. The trained network computes a reference for reconstruction errors, which involves the mean squared error between the input and output for each sensor. This reference serves as the intact model reference, representing the undamaged structural condition.

Damage detection evaluation Cracks are randomly introduced in various locations in the finite element model. To simulate crack propagation, each damage scenario involves an increase in the crack length l from 4mm to 60mm , while keeping the crack width w and orientation (angle) α fixed. An example of the damaged plates and the meshing is illustrated in Fig. 2c. As the compressed sensor data are now collected from the damaged plate, small batches of data sets are fed into the trained

model for evaluation and to generate a set of testing reconstruction errors. To showcase the damage detection mechanism, these errors are compared to the reference reconstruction errors from baseline behavior. The pattern of the reconstruction error distributions can reveal how close the response behavior of the testing structure resembles the original undamaged system. Additionally, it is worth noting that the number of anomaly data samples is limited to 20 or less to demonstrate the rapid damage detection capabilities. This makes the method efficient, useful, and applicable on actual testing sites for near real-time damage detection.

In Fig. 2d, we present histogram distributions comparing the undamaged baseline to the damaged structure with varying crack lengths. In the case of minor damages (8mm), the testing reconstruction errors show overlap with the undamaged reconstruction error reference. This overlap suggests a similarity in structural response behavior with minor separation in the distributions. As the damage grows, for a 20mm crack, noticeable differences emerge in the histogram distributions between the testing reconstruction errors and the undamaged reference. These disparities indicate that the model cannot accurately reconstruct the dataset due to the presence of anomalies, and that implements the detection principle. Furthermore, with the continuing increase in crack length (40mm), the distribution of testing reconstruction errors shifts toward higher magnitudes. In this case, the damage within the structure is very easily detected.

To further expand on damage detection performance, the proposed Mechanics-AE is evaluated against standard autoencoders using a range of classification metrics, including accuracy, precision, F1-score, and area under the receiver operating characteristic (AUROC) [47] (Detailed information on calculating the detection metrics is provided in the Method Section). Figure 2e demonstrates that Mechanics-AE outperforms the autoencoders in all five metrics across different ranges of crack lengths. Additionally, it is crucial to emphasize that the performance of the autoencoders exhibits considerable variability when tested on different samples, whereas Mechanics-AE consistently delivers more stable and robust results. Furthermore, Mechanics-AE exhibits significant improvement in detection performance even at the early crack propagation stage (before 2mm), which is very crucial for early detection in real applications, especially on fracture critical structural components that typically lack a baseline model and exhibit a unique behavior even for similarly designed components.

Detection performance comparison with other ML methods The damage detection performance is comprehensively evaluated through a comparison with four baseline methods: Isolation Forest [48], One-Class support vector machines (OCSVM), LODA [49], and autoencoders. Sensor data from small (15mm), medium (30mm), and large (40mm) crack lengths are utilized for

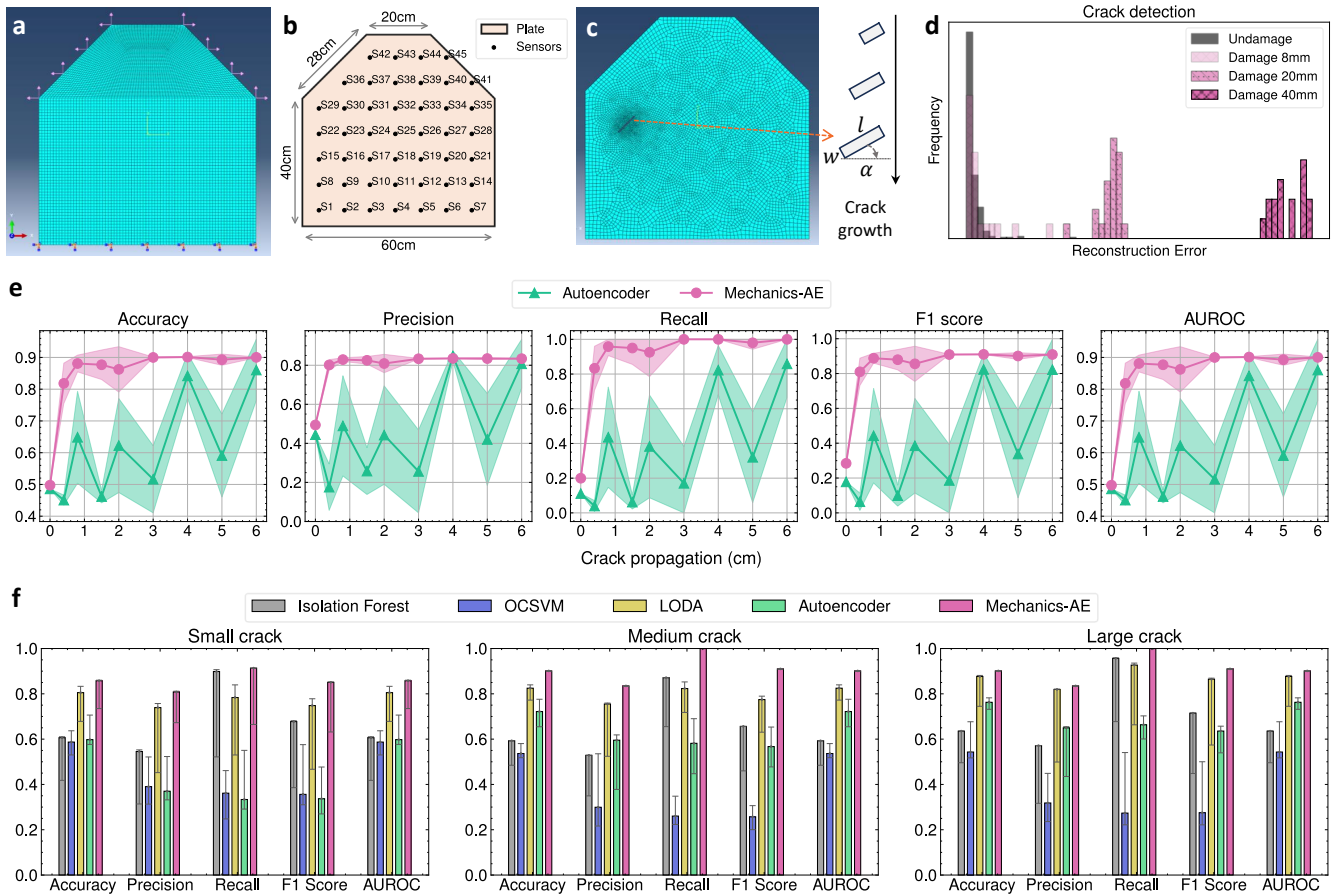


FIG. 2. Damage detection of a cracked plate. **a**, Finite element setup, with the mesh of the intact gusset plate, boundary conditions, and loading. **b**, Sensor distribution and labels. **c**, A typical cracked plate and its meshing. Different crack lengths represent damage progression. **d**, The distributions of reconstruction errors from undamaged structure reference and three different damaged scenarios. As damage propagates, the distribution shifts to the right and becomes distinct from the undamaged reference. **e**, Damage detection performance as the crack propagates. Compared to the baseline autoencoder, Mechanics-AE exhibits higher values in all five metrics, especially in the early stages of the crack growth. **f**, Performance comparison between various anomaly detection methods at three typical crack lengths. Mechanics-AE consistently achieves higher damage detection rates compared to other baseline methods.

analysis. Here, we extensively evaluate 37 cases with different crack locations and crack widths. In Fig. 2f, the results demonstrate that Mechanics-AE consistently surpasses all other methods in terms of accuracy, recall, F1-score, and AUROC. Additionally, when compared to standard autoencoders, the incorporated mechanics knowledge in Mechanics-AE demonstrates significant enhancement, particularly in small crack scenarios.

Damage localization evaluation Furthermore, Mechanics-AE showcases a robust capability in accurately localizing damages, even when the damage is relatively small. The localization process is distinct from the detection process that involves computing reconstruction errors. In the localization process, we evaluate the differences between the network input norms of $\|\mu\|$ and $\|\sigma\|$ with the corresponding output norms from each sensor. Subsequently, the differences obtained from the training

reference and testing are further compared to derive a damage score, denoted as p (refer to the Method Section for specifics). A high score indicates the presence of damage adjacent to that sensor. As damage scores vary among sensors, the contour based on the scores and sensors' locations can efficiently pinpoint damages.

Figure 3a illustrates the damage localization contours among different crack lengths at the same damage location. The grey background in the graph represents the plate geometry, while the inner contour is plotted based on the scores. In the first row, the intact structure exhibits a uniform color with no peak values, indicating the absence of detected damage. As damage propagates, Mechanics-AE accurately localizes a medium-size crack (20mm), as indicated by a sensor adjacent to the crack displaying a peak magnitude highlighted in yellow. As the crack continues to propagate to a large-size crack

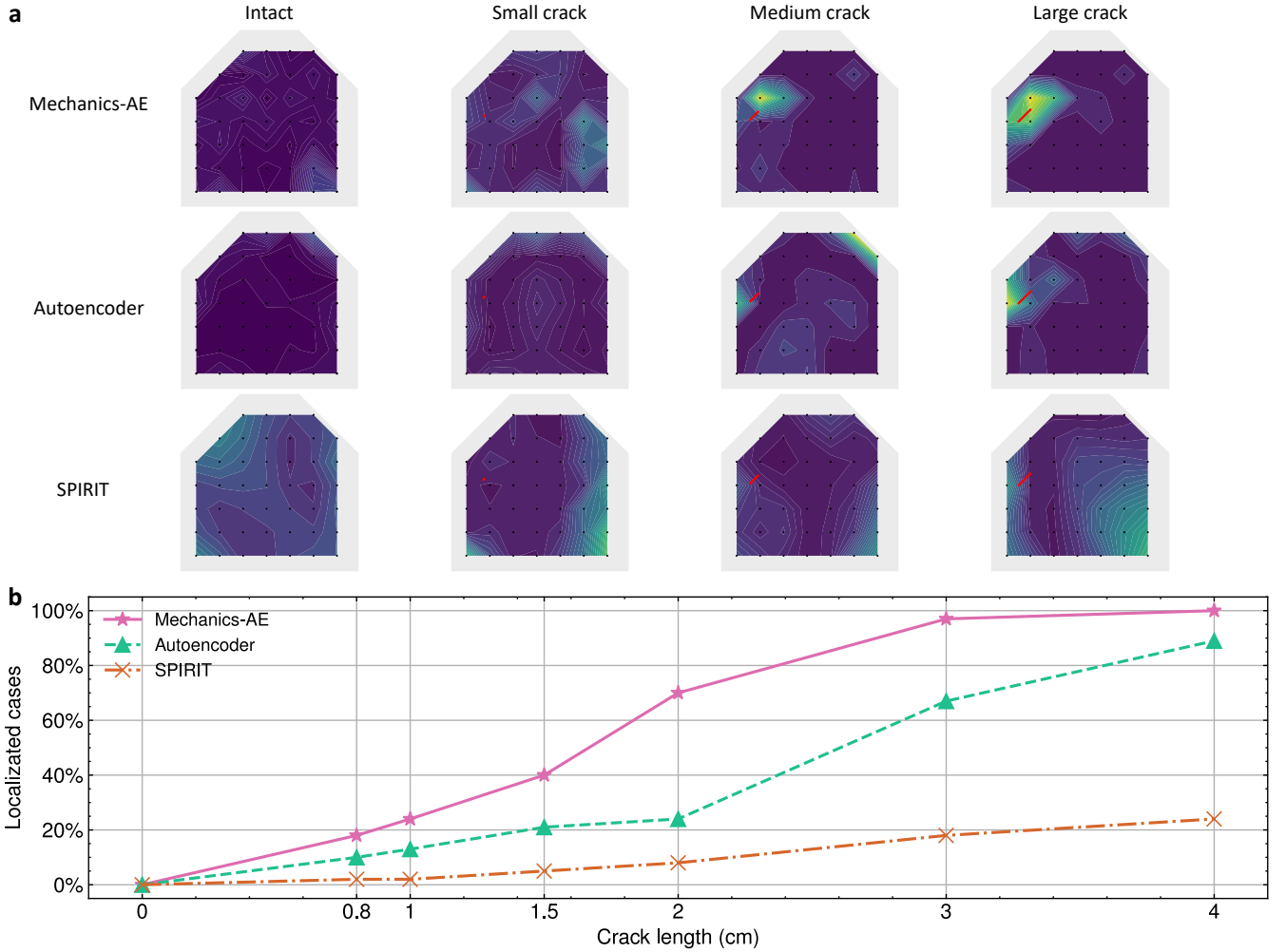


FIG. 3. Comparison of damage localization performance as crack propagates. The proposed Mechanics-AE can localize crack in earlier stages of the crack propagation compared to other methods. **a**, Damage localization contour of a crack scenario. The successful localization is determined by whether one or more sensors near the crack display a yellow color (peak values in the contour). Compared to SPIRIT and autoencoder, Mechanics-AE can localize the crack earlier at a medium crack level. **b**, Early damage localization performance. An extensive analysis of 37 different crack scenarios is conducted, and the y axis refers to the percentages of cases which damages are successfully localized. Compared to autoencoder and SPIRIT, Mechanics-AE exhibits a higher success rate in early localization as cracks propagate. On average, Mechanics-AE localizes the damage 11mm earlier than the standard Autoencoder method, which is relatively a 35% reduction in terms of the crack length.

(40mm), the contour's yellow color precisely overlays the crack region, providing a visually enhanced localization. Furthermore, compared to the other two baseline methods (in the second and third rows of Fig. 3a), autoencoder and SPIRIT [50, 51], Mechanics-AE is capable of localizing damages at an earlier stage (20mm) during crack propagation. It is also worth noting that when testing the small crack scenario, the presence of yellow colors near the structural boundaries may not conclusively indicate the correct crack location because structural response variations in those areas are typically larger. Despite this, the damage scores are still higher than the undamaged reference, and the contour still indicates the presence of certain damages within the structure.

In addition, damage localization is carried out for the same 37 cases mentioned in the detection evaluation. Figure 3b demonstrates the localization performance of Mechanics-AE autoencoder, and SPIRIT by evaluating their success in localizing the damage across these 37 cases at different crack lengths. Compared to autoencoder and SPIRIT, Mechanics-AE demonstrates an overall higher success rate and an average of 35% earlier localization in terms of the crack length. Also, Mechanics-AE can localize most of the cracks at the size of 30mm while the autoencoder still fails in many cases. Damage localization results for other cases are displayed in Supplementary Fig. 1, and the process for damage detection and localization is displayed in Supplementary Movie 1.

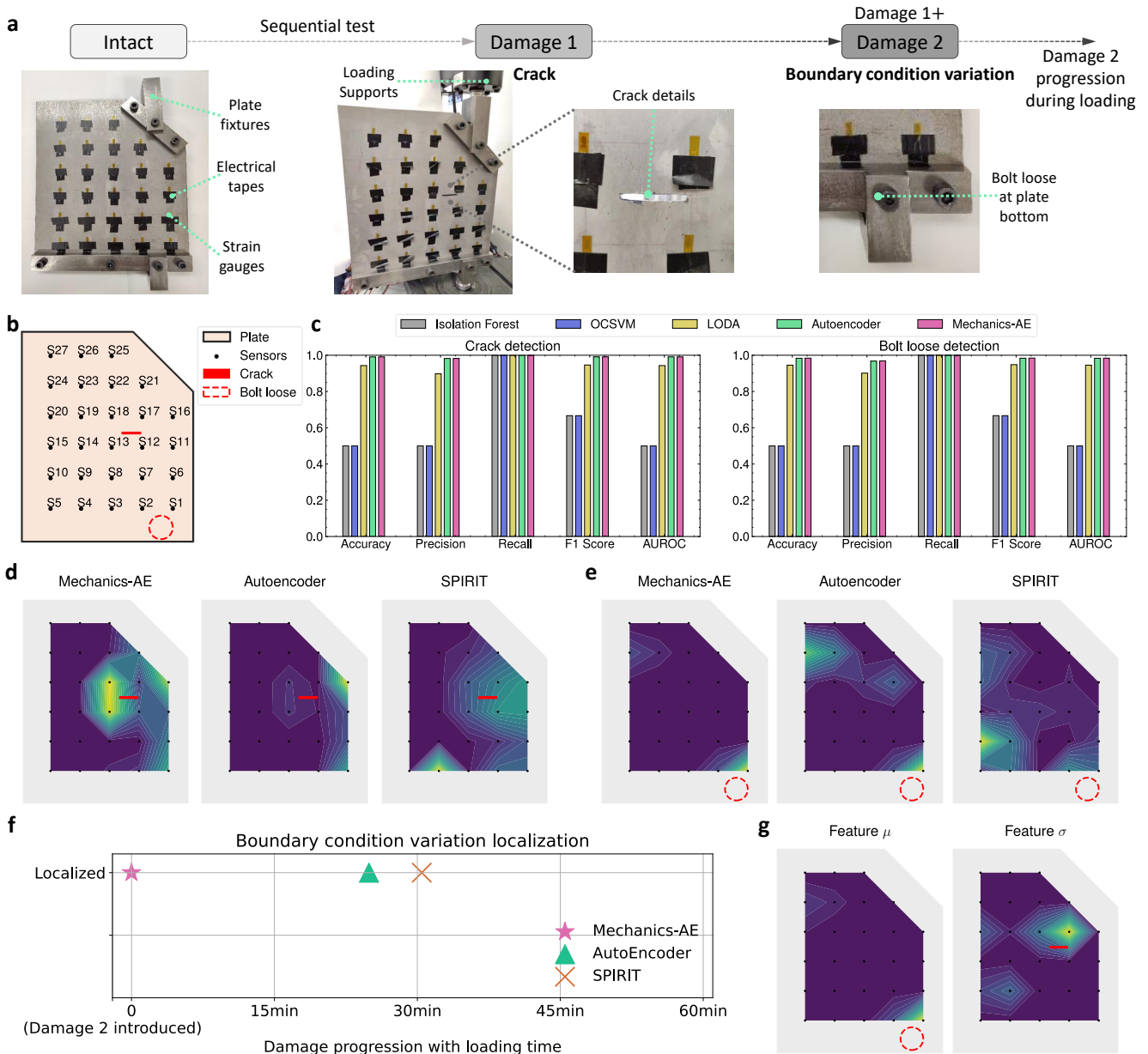


FIG. 4. Experimental work of early damage detection and localization on a steel plate structure. **a**, The experimental setup for the plate. Two types of damage are introduced sequentially (a crack and boundary condition variation). The crack is located in the middle of the plate, and the second damage is introduced through loosening the bolt connections. While under loading, the connection of the plate gradually loosens, representing the growth of damage. The strain sensors are evenly distributed and deployed on the plate. The plate is fixed with top and bottom fixtures for loading. **b**, The details of two damage locations and the locations of the sensors. **c**, The damage detection performance for the crack and the boundary condition variation. **d**, The crack localization results. Mechanics-AE delineates the crack region with yellow color (peak area) surrounding the crack tips, which is more accurate than the autoencoder for localization. SPIRIT fails to localize the damage. **e**, The localization results for the boundary condition scenario at 20min loading after introducing the damage 2. Only Mechanics-AE can localize the damage at the bottom plate connection at the early loading stage (damage growth). **f**, Localization performance for boundary condition variation. In comparison to autoencoder and SPIRIT, Mechanics-AE can early localize the variations in boundary condition once the damage is introduced. As damage 2 continues to propagate during loading, both the autoencoder and SPIRIT gradually succeed in localizing the damage. **g**, Damage differentiation with contours based on compressed sensor features μ and σ . μ feature is more associated with boundary condition changes and σ feature corresponds more to the crack.

Experimental validations We evaluate the proposed Mechanics-AE on a plate structure (Fig. 4a) to demon-

strate the method's feasibility. The experimented steel plate measures approximately 45cm \times 36cm, and 27

strain sensors are attached to the plate surface with a center-to-center gap of 6.5cm . Random traffic-like loading is applied to the intact plate structure for 3 hours to generate enough data for the neural network training. Subsequently, damage is introduced to the plate. To demonstrate the ability to differentiate between damage types, we opt to sequentially evaluate two typical types of damage—cracks followed by boundary condition variations—applied on the plates during the experiment. This approach allows us to illustrate a progression of damage. As shown in Fig. 4a, the first damage, a crack of size $4\text{cm} \times 0.5\text{cm}$ is introduced at the middle right side of the plate. Next, the second type of damage (boundary condition variations) is also displayed at the lower boundary connection of the plate. The damage is introduced by manually loosening the connection of the plate to the loading frame. The connection continues to loosen throughout the experimental loading, illustrating the progression of the boundary condition damage. In both damage states, random traffic loading is applied to the plate before and after introducing damage, and corresponding strain response data are recorded from all sensors. Subsequently, data from damaged structures undergo evaluation using the same procedure as in the finite element simulation. Figure 4b displays the detailed sensor deployment and the two damage locations.

Next, Mechanics-AE is demonstrated to detect and localize those unseen damages, whether a crack or a variation in boundary conditions. In Figure 4c, damage detection for both scenarios is examined with Isolation Forest, One-class Support Vector Machines (OCSVM), LODA, autoencoders, and Mechanics-AE. Results show that, for the introduced large damages, Mechanics-AE performances is on par compared to the autoencoder, but still surpasses other baseline methods. Mechanics-AE is advantageous in accuracy for small damage variations.

Figure 4d presents the crack localization contours. Compared to the standard autoencoder, the integrated mechanics knowledge significantly improves the damage localization accuracy. The contour exhibits a much larger peak region on both sides of the crack. This occurs because stress concentration primarily takes place at the tips of the crack, and the sensors located on both sides of the crack’s tip sense the structural response variations. In comparison, the autoencoder contour exhibits a similar pattern but only displays a very faint yellow color near the right side of the crack tip. However, its magnitudes are relatively minor and may not provide robust evidence for more precise damage localization. This suggests that our proposed method is more sensitive to minor damages, enlarging such discrepancies and providing improved localization contours compared to the standard autoencoder. Meanwhile, SPIRIT failed to localize the crack.

Figure 4e showcases the damage localization contours for the boundary condition variation for the first 2min

loading after manually loosening the plate connections (introduce damage 2). Only Mechanics-AE can successfully pinpoint the anomalies at the bottom right corner of the plate. This region corresponds to the actual location of boundary variations introduced. Autoencoder and SPIRIT exhibit lower localization performance with late localization during damage progression. Figure 4f shows the progression of damage localization among different methods. Autoencoder and SPIRIT can only localize the damage after 20min of loading. This once again demonstrates that Mechanics-AE exhibits higher sensitivity, enabling early localization of damage. The detailed mechanism is further specified in Supplementary Fig. 2. Overall, we have demonstrated that Mechanics-AE achieves early detection and localization for different types of damages.

Damage differentiation In addition to damage detection and localization, Mechanics-AE can also distinguish unseen types of damage based on the compressed sensor data features μ and σ . We independently evaluate the features μ and σ derived from the Gaussian distribution by directly computing the norm errors. Figure 4g presents two distinct contours derived from sensor features μ and σ . The analysis demonstrates that feature μ , representing the average value of the strain responses, is more closely associated with the boundary condition variations. This association is attributed to the fact that the loosening of structural connections reduces the structure’s stiffness, resulting in an overall decrease in strain magnitudes. On the other hand, the σ (standard deviation) contour is more related to the cracks induced by stress concentrations. Sensors positioned near the crack tips display elevated strain values during loading, leading to increased variations (an increase in standard deviation) among the strain response. In Supplementary Fig. 4, additional results are displayed regarding distinguishing different types of damage.

DISCUSSION

In this paper, we presented Mechanics-AE for automated detection and localization of unforeseen damages, as well as the differentiation between different types of damage. Mechanics-AE leverages the sensor relationships based on mechanical strain response, enhancing not only the performance of anomaly detection during early damage growth but also enabling earlier damage localization compared to other methods. Sensors positioned at various locations gather time-series data from an intact structure. This data is subsequently compressed into different sensor features and employed for autoencoder network training. This allows the model to learn the reference from the intact structural condition, aiding in capturing anomalies indicative of structural damages. The proposed Mechanics-AE requires only a minimal amount

of data samples for damage detection and localization. Furthermore, Mechanics-AE outperforms standard machine learning techniques like One-Class SVM, Isolation Forest, and LODA in datasets from two damaged scenarios. Mechanics-AE surpasses these methods by achieving higher accuracy, precision, recall, F-score, and AU-ROC, indicating its superior performance in detecting and classifying anomalies. Additionally, the introduced novel loss function greatly facilitates damage localization by incorporating structural responses from sensor placement. Results demonstrate that incorporating the added loss function can effectively localize various damages in numerical and experimental structural experiments. The use of this loss function helps localize the occurrence of damages in the early stage of damage propagation, up to 35% earlier. Laboratory experiments also indicate the model’s capability to distinguish between different types of damage (boundary condition variations and cracks) in gusset plate structures. Future work can focus on experimenting on larger scale structures, sensor placement optimization, and fine-tuning the mechanics correlations between different sensors.

METHODS

Finite element analysis (FEA) The gusset plate is simulated using 3D elements (C3D8R) in ABAQUS under clamped-clamped boundary conditions at the bottom edge of the plate. The Poisson ratio and Young’s modulus are 0.32 and $200GPa$, respectively. To simulate traffic loading, random loading magnitudes are applied to the top left and top right edge in both $-x$ and $-y$ directions. The loading magnitudes are defined as periodic data generated by 100 combinations of Sine and Cosine functions. Each function has a different combination of random phase, frequency, and peak amplitude drawn from normal distributions.

To generate enough training data, the FEA of the undamaged plate structure are repeated with different random loads for multiple iterations. In the cases of damaged structures, random cracks are introduced within the plate geometry, varying in location, length (l), width (w), and angle (α). Notably, the mesh size is set to $0.2cm$ for the crack area and $1cm$ for all other regions. The strain responses are obtained by averaging the values across all elements within the specified sensor regions.

Data compression and dataset construction In this study, it is assumed that N sensors have been affixed to the structure of interest at N locations. During normal operation, the structure experiences continuous loading forces of unknown magnitude. Each sensor S_i continuously measures a strain signal ε_i over time (where $i = 1, 2, \dots, N$).

The data reduction approach is mainly adopted from [52, 53] to solve large data problems typically generated

from structural monitoring sensors (see Fig. 5a). The approach can be summarized as follows: (i) predefining several strain thresholds based on the overall strain events, (ii) calculating the cumulative times for a selected segment of strain-time responses for all levels of the threshold, (iii) fitting the cumulative time data to the Gaussian equation 1 for data compression, and (iv) obtaining the parameters for Gaussian cumulative density function (CDF) through equation 1.

$$F_{Gaussian}(\varepsilon) = \frac{A}{2} \left[1 - erf\left(\frac{\varepsilon - \mu}{\sigma\sqrt{2}}\right) \right] \quad (1)$$

where A is the summation of all cumulative time events. μ and σ represent the mean and standard deviation of the cumulative density function, and erf denotes the Gauss error function. To determine the thresholds in Fig. 5a, the mean strain value ε_{mean} is computed by averaging the strain responses collected from all sensors in the undamaged structure. Then, the seven threshold values are evenly distributed between $0.5\varepsilon_{mean}$ and $3\varepsilon_{mean}$. For each sensor, every 200 data points are compressed into one set of μ and σ (see Fig. 5b).

Next, the compressed sensor data μ and σ (see right side of Fig. 5b) are utilized to construct the dataset in batches. We use a moving window with length $l = 12$ and a stride of 2 to construct one batch. For example, the first training sample is taken from the 1st to the 12th segment, the second training sample is from the 3th to the 14th segment, then from the 5th to the 16th segment. The constructed dataset has a size of $B \times l \times 2N$ that represents the number of batches, time-series data length, and the number of sensor parameters μ and σ , respectively.

Mechanics-AE network Figure 5c illustrates the architecture of the presented mechanics autoencoder neural network. Specifically, the input and output have the same matrix size, with the output designed to reconstruct the input values. The first part of the loss function is computed as the summation of the mean squared error (MSE).

$$\mathcal{L}_{MSE} = \frac{1}{n} \sum (\mathbf{y} - \mathbf{x})^2 \quad (2)$$

where n , \mathbf{x} , and \mathbf{y} denote the number of samples, the input, and the output from the neural network, respectively.

To further enhance the method by leveraging the knowledge of structural mechanics, it is important to take into account the correlation of strain changes between two adjacent points in an undamaged structure. These mechanical characteristics can be incorporated into the neural networks by considering the sensors’ mechanical responses. As shown in Fig. 5d, the mechanics loss is evaluated for every pair of sensors i and j . The mechanics loss term $\mathcal{L}_{Mechanics}$ and the proposed loss function \mathcal{L} can be calculated using the following equations.

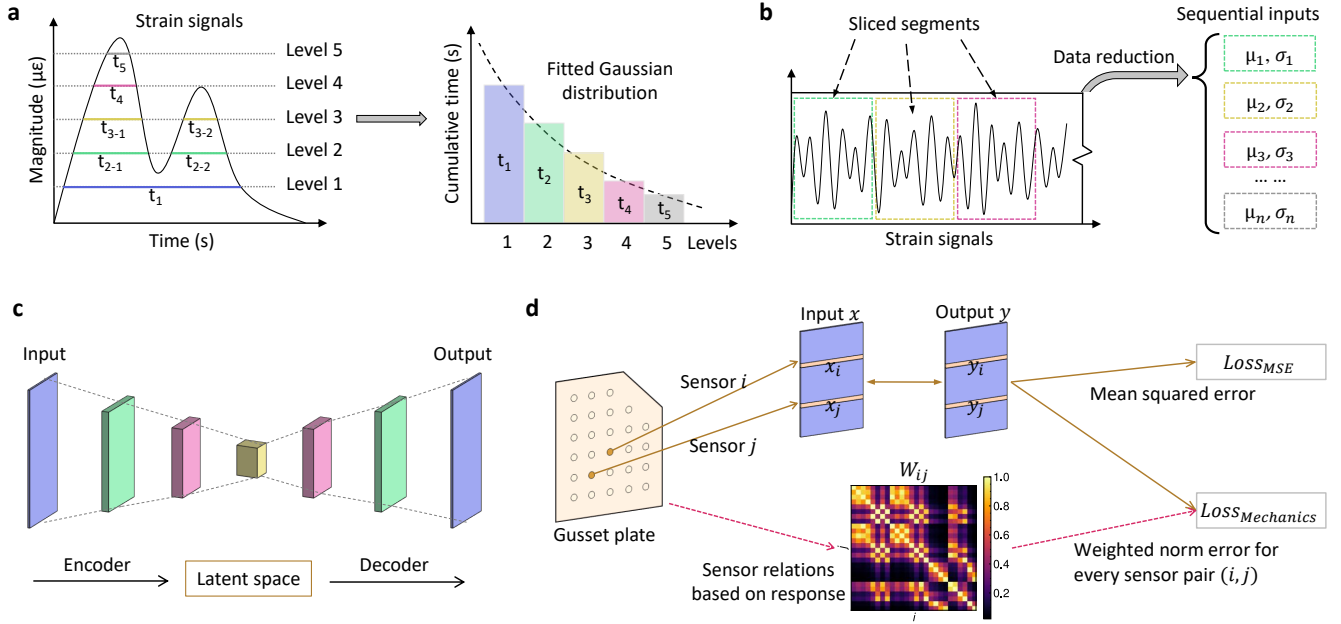


FIG. 5. Mechanics-AE methodology. **a**, Sensor data compression algorithm based on Gaussian distribution. In the left graph, time-series sensor responses from structures are recorded, and different threshold levels are defined based on the overall response magnitudes. Next, cumulative events above each threshold level are computed and plotted in the second graph, which is supposed to follow a Gaussian distribution. The best combination of μ and σ is obtained as the compressed sensor data through curve fitting. **b**, Sensor data processing and dataset construction. **c**, An autoencoder neural network architecture. **d**, The proposed loss function. The weight matrix is computed based on the strain responses from each pair of sensors. Values are shown as a contour in the lower part of the graph.

$$\mathcal{L}_{Mechanics} = \sum_{i,j} W_{ij} (\Delta_i - \Delta_j)^2 \quad (3)$$

$$\Delta_i = \| \mathbf{y}_i \| - \| \mathbf{x}_i \| \quad (4)$$

$$W_{ij} = \begin{cases} \max(\varepsilon_i) / \max(\varepsilon_j), & \text{if } \max(\varepsilon_i) < \max(\varepsilon_j) \\ \max(\varepsilon_j) / \max(\varepsilon_i), & \text{if } \max(\varepsilon_i) \geq \max(\varepsilon_j) \end{cases} \quad (5)$$

$$\mathcal{L} = \mathcal{L}_{MSE} + \gamma \mathcal{L}_{Mechanics} \quad (6)$$

where Δ_i refers to the norm difference of the input and output at sensor i , and Δ have shapes of $n \times l \times 2N$. \mathbf{x}_i and \mathbf{y}_i represent the corresponding input and output of the neural network from sensor i . The norm operation in equation 4 is evaluated in the time-series dimension (2^{nd} dimension). W denotes the weight matrix defined based on each sensor's strain responses, with all element values less than or equal to 1. It is worth noting that W is calculated based on the original strain responses. γ serves as the penalty coefficient for mechanics loss term and is fine-tuned to 0.05 in this study. The proposed model, trained on equation 6, enhances the characteristics of structural

integrity and model predicting sensitivity. Specifically, a dataset from the damaged structure will not follow the original mechanical features from the intact structure, resulting in poor reconstruction by the neural network and higher reconstruction errors.

Damage detection metric After training, the model utilizes the training reconstruction errors $\hat{\Gamma}$ as a reference and compares to the testing reconstruction errors Γ to identify any deviations in the distribution of testing samples. Assuming there are m testing samples from N sensors; the input, output, and reconstruction error would have $m \times N$ values. The reconstruction error Γ for each data point is calculated as:

$$\Gamma_i^j = (y_i^j - x_i^j)^2 \quad (7)$$

where $j = 1, 2, \dots, m$ and $i = 1, 2, \dots, N$.

To assess the damage detection performance, all testing data Γ (size of $m \times N$) are first categorized as either anomaly (positive) or normal data (negative). This classification is accomplished by setting adaptive thresholds based on false positive rates (FPR) derived from training reconstruction errors. Next, we define a ratio q to ascertain whether a testing sample originates from a damaged structure, across all m samples. Specifically, if more than $q * N$ of the N sensors were previously classified as

anomalies, the sample is deemed to originate from a damaged structure. As a result, all m testing samples predict whether the structure is damaged, providing the feasibility to calculate various metrics later on. It is important to highlight that due to a limited number of testing data, SMOTE [54] is employed to up-sample them to the same quantity as the undamaged dataset. Subsequently, sample predictions are compared to the ground truth using binary classification metrics, including accuracy, precision, recall, F1-score, and AUROC.

Damage localization metric Damage can be accurately localized by comparing the obtained norm error Δ from equation 4 across different sensors. In detail, the objective is to calculate the damage condition at each sensor as a single value, and this computation is divided into two steps. First, $\hat{\Delta}$ calculated from the undamaged data and Δ calculated from damaged testing data are compared with the reference, considering each sensor parameter μ or σ . This intermediate term is denoted as \mathcal{T} as shown in equation 8, representing the relative changes of reconstruction errors. Second, \mathcal{T} from two types of parameters (μ and σ), are integrated as a single metric for conciseness. Therefore, the damage score p is introduced as a damage estimation metric in equation 9.

$$\mathcal{T} = \frac{\left| \frac{1}{m} \sum \Delta - \frac{1}{n} \sum \hat{\Delta} \right|}{\frac{1}{n} \sum \|x\|} \quad (8)$$

$$p = \left(\lambda \frac{\mathcal{T}^\mu}{\max(\hat{\mathcal{T}}^\mu)} + (1 - \lambda) \frac{\mathcal{T}^\sigma}{\max(\hat{\mathcal{T}}^\sigma)} \right) / 2 \quad (9)$$

where in the first equation, $\frac{1}{m} \sum \Delta$ estimates the mean value from all m testing samples, $\frac{1}{n} \sum \hat{\Delta}$ represents the mean value from all n training samples, and the denominator $\frac{1}{n} \sum \|x\|$ calculates the average of the corresponding norm. In the second equation, \mathcal{T}^μ and \mathcal{T}^σ are vectors of relative parameter errors from parameters μ and σ based on sensors, respectively. $\hat{\mathcal{T}}^\mu$ and $\hat{\mathcal{T}}^\sigma$ are the corresponding $\hat{\mathcal{T}}$ calculated from the reference. λ is a coefficient that leverages the contribution from parameters μ and σ to damage score p . In this work, λ is set to 0.5 for simulations and 0.2 for experiments.

The proposed estimation function can effectively differentiate the undamaged and damaged regions based on the damage scores. Specifically, a damage score p less than 1 represents the baseline or the undamaged case, while a higher score demonstrates damages around the sensor region. To some extent, the magnitude of p can indicate the damage severity at the corresponding sensor location. However, such a pattern is not consistently observed when the damage is small. Furthermore, by incorporating the location information of all sensors and the p scores, the analysis can establish contours for more precise localization of structural damages and estimate the overall structural integrity.

The baseline localization method SPIRIT is also named streaming pattern discovery in multiple time series. SPIRIT uses incremental PCA to find correlations and hidden variables that summarize the trend and signify pattern changes. The projection coefficients (i.e., W_1 and W_2 of the PCA weight matrix W) of the first two hidden variables are computed for both the training and testing datasets. The damage scores p are calculated as the element-wise Euclidean distance between the training data point ($W_{i,1}^{train}, W_{i,2}^{train}$) and test data point ($W_{i,1}^{test}, W_{i,2}^{test}$) where $i = 1, 2, \dots, n$. The corresponding norm error Δ for SPIRIT can be calculated as the element-wise Euclidean distance using equation 10, while the damage score will be computed as in equation 9 above.

$$\Delta = \sqrt{(W_{i,1}^{train} - W_{i,1}^{test})^2 + (W_{i,2}^{train} - W_{i,2}^{test})^2} \quad (10)$$

Laboratory experiment setup For laboratory experiment, the Young's modulus of the testing steel plate is unknown. The strain gauge type is 1-LY11-6/350 and is attached vertically to measure the strain in the vertical direction, aligning with the vertically applied loading. The clamped-clamped boundary conditions of the plate are considered due to their higher controllability in an experimental setup, compared to other types of boundary conditions, such as pinned-pinned or pinned-clamped.

A continuous random simulated traffic effect loading profile is generated with a time step of 0.1s. Displacement-control testing is performed using an MTS loading frame model, applying the loading at the top and bottom fixtures. The strain sensors are connected to a NI-9236 strain input module for strain responses monitored during the loading stage, and the raw strain data is collected through LabVIEW. For data compression, 7 threshold levels are selected, ranging from 30 to 175 $\mu\epsilon$ with an increment of 24 $\mu\epsilon$.

Data availability The numerical simulation and experimental data supporting the findings of this study are available for reference. The data is available at <https://github.com/human-analysis/anomaly-detection-shm>.

Code availability The codes are provided along with the data at <https://github.com/human-analysis/anomaly-detection-shm>.

Acknowledgement This study was partially supported by the National Science Foundation Award CNS 1645783.

Author contributions N.L. and V.B. supervised the study. X.L., N.L., and V.B. conceived the initial idea and contributed to machine learning. X.L. and H.B. performed finite element analysis and the case studies. H.B. contributed to the setup of the laboratory experiment and preprocessed the data. T.S. and X.L. performed all laboratory experiments and data collection. X.L. and M.M. contributed to Supplementary Information. X.L., M.M., N.L., and V.B. wrote the paper.

Competing interests The authors declare no competing interests.

Correspondence and requests for materials should be addressed to vishnu@msu.edu and lajnefni@msu.edu.

-
- [1] S. Pezeshk, C. V. Camp, A. Kashani, M. Akhiani, *et al.*, Data analyses from seismic instrumentation installed on the i-40 bridge, Tennessee. Department of Transportation (2021).
- [2] H. Carnahan, Pittsburgh bridge collapse emphasizes need for bridge repairs, *Journal of Protective Coatings & Linings* **39**, 6 (2022).
- [3] L. Capineri and A. Bulletti, Ultrasonic guided-waves sensors and integrated structural health monitoring systems for impact detection and localization: A review, *Sensors* **21**, 2929 (2021).
- [4] Z.-F. Tang, X.-D. Sui, Y.-F. Duan, P.-f. Zhang, and C. B. Yun, Guided wave-based cable damage detection using wave energy transmission and reflection, *Structural Control and Health Monitoring* **28**, e2688 (2021).
- [5] C. J. Lissenden, Y. Liu, and J. L. Rose, Use of nonlinear ultrasonic guided waves for early damage detection, *Insight-Non-Destructive Testing and Condition Monitoring* **57**, 206 (2015).
- [6] N. Chandarana, D. M. Sanchez, C. Soutis, and M. Gresil, Early damage detection in composites during fabrication and mechanical testing, *Materials* **10**, 685 (2017).
- [7] S. Song, X. Zhang, Y. Chang, and Y. Shen, An improved structural health monitoring method utilizing sparse representation for acoustic emission signals in rails, *IEEE Transactions on Instrumentation and Measurement* **72**, 1 (2022).
- [8] M. H. Daneshvar, A. Gharighoran, S. A. Zareei, and A. Karamodin, Early damage detection under massive data via innovative hybrid methods: application to a large-scale cable-stayed bridge, *Structure and Infrastructure Engineering* **17**, 902 (2021).
- [9] N. Bakhary, H. Hao, and A. J. Deeks, Substructuring technique for damage detection using statistical multi-stage artificial neural network, *Advances in Structural Engineering* **13**, 619 (2010).
- [10] M. Betti, L. Facchini, and P. Biagini, Damage detection on a three-storey steel frame using artificial neural networks and genetic algorithms, *Meccanica* **50**, 875 (2015).
- [11] Z. Li, W. Lin, and Y. Zhang, Real-time drive-by bridge damage detection using deep auto-encoder, in *Structures*, Vol. 47 (Elsevier, 2023) pp. 1167–1181.
- [12] H. Hasni, A. H. Alavi, P. Jiao, N. Lajnef, K. Chatti, K. Aono, and S. Chakrabartty, A new approach for damage detection in asphalt concrete pavements using battery-free wireless sensors with non-constant injection rates, *Measurement* **110**, 217 (2017).
- [13] A. Esfandiari, M.-S. Nabiyan, and F. R. Rofooei, Structural damage detection using principal component analysis of frequency response function data, *Structural Control and Health Monitoring* **27**, e2550 (2020).
- [14] Y.-L. Xu, J.-F. Lin, S. Zhan, and F.-Y. Wang, Multi-stage damage detection of a transmission tower: Numerical investigation and experimental validation, *Structural Control and Health Monitoring* **26**, e2366 (2019).
- [15] N. S. Gulgec, M. Takáč, and S. N. Pakzad, Convolutional neural network approach for robust structural damage detection and localization, *Journal of computing in civil engineering* **33**, 04019005 (2019).
- [16] S. Mustafa, H. Sekiya, and S. Hirano, Evaluation of fatigue damage in steel girder bridges using displacement influence lines, in *Structures*, Vol. 53 (Elsevier, 2023) pp. 1160–1171.
- [17] X. Li, T. Salem, H. Bolandi, V. Boddeti, and N. Lajnef, Methods for the rapid detection of boundary condition variations in structural systems, in *Smart Materials, Adaptive Structures and Intelligent Systems*, Vol. 86274 (American Society of Mechanical Engineers, 2022) p. V001T05A004.
- [18] B. Wu, G. Wu, C. Yang, and Y. He, Damage identification method for continuous girder bridges based on spatially-distributed long-gauge strain sensing under moving loads, *Mechanical Systems and Signal Processing* **104**, 415 (2018).
- [19] T. Li, Z. Wang, S. Liu, and W.-Y. Lin, Deep unsupervised anomaly detection, in *Proceedings of the IEEE/CVF Winter Conference on Applications of Computer Vision* (2021) pp. 3636–3645.
- [20] G. Heo, C. Kim, S. Jeon, and J. Jeon, An experimental study of a data compression technology-based intelligent data acquisition (idaq) system for structural health monitoring of a long-span bridge, *Applied Sciences* **8**, 361 (2018).
- [21] S.-Z. Chen, G. Wu, and D.-C. Feng, Damage detection of highway bridges based on long-gauge strain response under stochastic traffic flow, *Mechanical Systems and Signal Processing* **127**, 551 (2019).
- [22] M. R. Azim and M. Gül, Data-driven damage identification technique for steel truss railroad bridges utilizing principal component analysis of strain response, *Structure and Infrastructure Engineering* **17**, 1019 (2021).
- [23] M. R. Azim and M. Gül, Development of a novel damage detection framework for truss railway bridges using operational acceleration and strain response, *Vibration* **4**, 422 (2021).
- [24] H. Hasni, A. H. Alavi, P. Jiao, and N. Lajnef, Detection of fatigue cracking in steel bridge girders: A support vector machine approach, *Archives of Civil and Mechanical Engineering* **17**, 609 (2017).
- [25] M. P. González and J. L. Zapico, Seismic damage identification in buildings using neural networks and modal data, *Computers & structures* **86**, 416 (2008).
- [26] D. Ma, H. Fang, N. Wang, B. Xue, J. Dong, and F. Wang, A real-time crack detection algorithm for pavement based on cnn with multiple feature layers, *Road Materials and Pavement Design* **23**, 2115 (2022).
- [27] M. Rautela and S. Gopalakrishnan, Ultrasonic guided wave based structural damage detection and localization using model assisted convolutional and recurrent neural networks, *Expert Systems with Applications* **167**, 114189 (2021).
- [28] D.-E. Choe, H.-C. Kim, and M.-H. Kim, Sequence-based modeling of deep learning with lstm and gru networks for structural damage detection of floating offshore wind turbine blades, *Renewable Energy* **174**, 218 (2021).
- [29] Z. Rastin, G. Ghodrati Amiri, and E. Darvishan, Unsupervised structural damage detection technique based on a deep convolutional autoencoder, *Shock and Vibration*

- 2021, 1 (2021).
- [30] F. Ni, J. Zhang, and M. N. Noori, Deep learning for data anomaly detection and data compression of a long-span suspension bridge, *Computer-Aided Civil and Infrastructure Engineering* **35**, 685 (2020).
- [31] F. Khoshnoudian, S. Talaei, and M. Fallahian, Structural damage detection using frf data, 2d-pca, artificial neural networks and imperialist competitive algorithm simultaneously, *International Journal of Structural Stability and Dynamics* **17**, 1750073 (2017).
- [32] S. Cao, H. Ouyang, and L. Cheng, Baseline-free adaptive damage localization of plate-type structures by using robust pca and gaussian smoothing, *Mechanical Systems and Signal Processing* **122**, 232 (2019).
- [33] D. Sen, K. Erazo, W. Zhang, S. Nagarajiah, and L. Sun, On the effectiveness of principal component analysis for decoupling structural damage and environmental effects in bridge structures, *Journal of Sound and Vibration* **457**, 280 (2019).
- [34] Z. Zhang and C. Sun, Structural damage identification via physics-guided machine learning: a methodology integrating pattern recognition with finite element model updating, *Structural Health Monitoring* **20**, 1675 (2021).
- [35] S. Zhang, C. M. Li, and W. Ye, Damage localization in plate-like structures using time-varying feature and one-dimensional convolutional neural network, *Mechanical Systems and Signal Processing* **147**, 107107 (2021).
- [36] S. Cofre-Martel, P. Kobrich, E. Lopez Droguett, and V. Meruane, Deep convolutional neural network-based structural damage localization and quantification using transmissibility data, *Shock and Vibration* **2019** (2019).
- [37] K. Jiang, Q. Han, X. Du, and P. Ni, A decentralized unsupervised structural condition diagnosis approach using deep auto-encoders, *Computer-Aided Civil and Infrastructure Engineering* **36**, 711 (2021).
- [38] J. P. Santos, C. Cremona, A. D. Orcesi, and P. Silveira, Early damage detection based on pattern recognition and data fusion, *Journal of Structural Engineering* **143**, 04016162 (2017).
- [39] J. P. Santos, C. Crémona, A. D. Orcesi, and P. Silveira, Multivariate statistical analysis for early damage detection, *Engineering Structures* **56**, 273 (2013).
- [40] C. Tutivén, Á. Encalada-Dávila, Y. Vidal, and C. Bernalcázar-Parra, Detecting bearing failures in wind energy parks: A main bearing early damage detection method using scada data and a convolutional autoencoder, *Energy Science & Engineering* **11**, 1395 (2023).
- [41] S. Sawant, A. Sethi, S. Banerjee, and S. Tallur, Unsupervised learning framework for temperature compensated damage identification and localization in ultrasonic guided wave shm with transfer learning, *Ultrasonics* , 106931 (2023).
- [42] M. Rautela, J. Senthilnath, J. Moll, and S. Gopalakrishnan, Combined two-level damage identification strategy using ultrasonic guided waves and physical knowledge assisted machine learning, *Ultrasonics* **115**, 106451 (2021).
- [43] H. Sohn, C. R. Farrar, F. M. Hemez, D. D. Shunk, D. W. Stinemas, B. R. Nadler, and J. J. Czarnecki, A review of structural health monitoring literature: 1996–2001, *Los Alamos National Laboratory, USA* **1**, 16 (2003).
- [44] S. M. Khan, S. Atamturktur, M. Chowdhury, and M. Rahman, Integration of structural health monitoring and intelligent transportation systems for bridge condition assessment: Current status and future direction, *IEEE Transactions on Intelligent Transportation Systems* **17**, 2107 (2016).
- [45] O. Abdeljaber, O. Avci, S. Kiranyaz, M. Gabbouj, and D. J. Inman, Real-time vibration-based structural damage detection using one-dimensional convolutional neural networks, *Journal of Sound and Vibration* **388**, 154 (2017).
- [46] Z. Wang and Y.-J. Cha, Unsupervised deep learning approach using a deep auto-encoder with a one-class support vector machine to detect damage, *Structural Health Monitoring* **20**, 406 (2021).
- [47] V. Bewick, L. Cheek, and J. Ball, Statistics review 13: receiver operating characteristic curves, *Critical care* **8**, 1 (2004).
- [48] F. T. Liu, K. M. Ting, and Z.-H. Zhou, Isolation forest, in *IEEE International Conference on Data Mining* (2008) pp. 413–422.
- [49] T. Pevný, Loda: Lightweight on-line detector of anomalies, *Machine Learning* **102**, 275 (2016).
- [50] S. Papadimitriou, J. Sun, and C. Faloutsos, Streaming pattern discovery in multiple time-series (Carnegie Mellon University, 2005).
- [51] I. Shafer, K. Ren, V. N. Boddeti, Y. Abe, G. R. Ganger, and C. Faloutsos, Rainmon: An integrated approach to mining bursty timeseries monitoring data, in *Proceedings of the ACM SIGKDD International Conference on Knowledge Discovery and Data Mining* (2012) pp. 1158–1166.
- [52] H. Bolandi, N. Lajnef, P. Jiao, K. Barri, H. Hasni, and A. H. Alavi, A novel data reduction approach for structural health monitoring systems, *Sensors* **19**, 4823 (2019).
- [53] H. Hasni, P. Jiao, N. Lajnef, and A. H. Alavi, Damage localization and quantification in gusset plates: A battery-free sensing approach, *Structural Control and Health Monitoring* **25**, e2158 (2018).
- [54] N. V. Chawla, K. W. Bowyer, L. O. Hall, and W. P. Kegelmeyer, Smote: synthetic minority over-sampling technique, *Journal of artificial intelligence research* **16**, 321 (2002).